Computer simulations of wetting of solid surfaces by liquid crystals

Andrew J. McDonald and Simon Hanna*
H.H. Wills Physics Laboratory, University of Bristol, Tyndall Avenue, Bristol, BS8 1TL, United Kingdom
(Received 31 May 2006; revised manuscript received 12 March 2007; published 18 April 2007)

Atomistic computer simulations are presented, consisting of droplets of model liquid crystal molecules wetting a generic crystalline surface. It is shown that the type of wetting that occurs is highly dependent on the value of the surface interaction parameter ε_{fs}, switching between partial wetting (no spreading) for $\varepsilon_{fs}=2.0$ to complete wetting for $\varepsilon_{fs}=2.5$. ε_{fs} is the multiplicative factor which scales the well depth of the fluid-surface interaction energy. During complete wetting, the spreading occurs through the growth of a precursor layer, and a set of secondary terraces. The temperature affects the structure of the droplet, as might be expected when different phases are sampled, and also the shape of the spreading droplet, and the rate of spreading. In particular, in the smectic-*A* phase at 350 K, for values of ε_{fs} just large enough to induce complete wetting, the precursor film assumes a diamond shape, with edges normal to the [110] directions in the crystal surface. It is shown that spreading occurs through diffusion across the surface, with the radius of the precursor layer increasing with the square root of time. Mass flow studies indicate that the spreading occurs by molecules cascading over the top of the droplet to feed the growing precursor layer. Calculations of contact angle relaxation are in qualitative agreement with experimental findings.

DOI: 10.1103/PhysRevE.75.041703 PACS number(s): 61.30.Hn, 61.30.Gd, 61.20.Ja

I. INTRODUCTION

In this paper we present a simulation study of *terraced wetting* of a liquid-crystal fluid on a solid surface. To model the liquid-crystal fluid we use the atomically detailed representation of 4-*n*-octyl-4′-cyanobiphenyl (8CB) developed previously [1].

The phenomenon of terraced wetting occurs when a fluid droplet completely wets a planar surface. As the droplet spreads radially, the macroscopic fluid edge is preceded by a microscopic "precursor film" which is comprised of a few molecular monolayers arranged in a characteristic "terraced" structure. The first monolayer, i.e., that closest to the surface, spreads most rapidly, followed by the next monolayer and so on. The macroscopic droplet acts as a reservoir, supplying fluid molecules to fuel the expansion of the terraced precursor film.

The "precursor film" mechanism was first observed in droplets of polydimethylsiloxane spreading on silicon wafers by Leger *et al.*, using ellipsometry [2]. Subsequent work by Heslot and Cazabat *et al.* enabled the analysis of the spreading profiles with submonolayer detail [3,4]. It was found that the precursor film was generally of a uniform thickness, corresponding to a single monolayer. However, under certain conditions, multiple terraces were observed, with the higher terraces also consisting of monolayers, but with smaller radii [3]. This finding contradicted the prevailing belief that droplets adopted a smooth "pancakelike" structure during spreading. It also suggested that any theory of complete wetting must take both short range forces and molecular dynamics into account.

It is possible to identify distinct terraced wetting regimes for "high-energy" and "low-energy" surfaces [4]. For high-energy surfaces, wetting occurs through the spreading of several monolayer terraces. On the other hand, only a single terrace or monolayer is observed for a low-energy surface. In both cases, the rate of radial spreading of the wetting monolayer was found to be proportional to the square root of time. Thus, the precursor film evolves over the surface in a diffusive manner, overcoming the liquid cohesion to behave like a two-dimensional gas. For this to occur, molecular anchoring to the surface must be negligible.

Since it was first discovered, considerable literature, both experimental and theoretical, has appeared concerning terraced wetting. Of particular note is a semicontinuum model proposed by de Gennes and Cazabat, which treats the monolayers as elastic sheets [5]. Other theoretical analyses have made use of molecular-kinetic theories of partial wetting to determine the dynamics of the contact angle [6–8].

Recently, experiments have been performed on the terraced wetting and spreading of liquid crystal systems [9,10]. Bardon *et al.* [9] observed "trilayers" as well as monolayers in the spreading of 8CB droplets on silicon substrates. The trilayers consisted of a smectic bilayer on top of a monolayer in which the molecules were tilted. The stability of the trilayer was thought to be due to the presence of electrostatic interactions between the molecules in adjacent layers. The authors analyzed spreading profiles over a range of temperatures finding that the trilayer configuration was always present. Experiments also reveal the presence of spreading trilayers in other *n*CBs, even those for which there is no smectic phase. From this, the authors conclude that the structure in the spreading terraces is not a direct reflection of the phase structure in the bulk system, but may in fact be induced by short-range forces and fluid-surface interactions.

A number of simulation studies have been performed on simple fluids, with the focus being to reproduce the "diffusive" dynamics of the precursor film radius $R(t)$, which is observed in experiment, and characterized by $R(t) \propto \sqrt{t}$. A series of simulations of simple atomic fluids [11–13] and light chain molecules [14] have demonstrated that registration of the fluid molecules with the surface is critical in de-

*Electronic address: S.Hanna@bristol.ac.uk

termining the spreading dynamics of the monolayer. A rough, atomically detailed surface, with atoms or molecules undergoing no significant penetration (absorption) was eventually shown to lead to "quasidiffusive" spreading of the monolayer and the experimentally observed spreading dynamics [15].

Coarser-grained models have also been used to study wetting phenomena. For example, Müller *et al.* have examined the wetting of smooth surfaces using Gay-Berne particles, and concluded that there is no evidence of a first order prewetting transition in this system [16].

The simulation of anisotropic fluids undergoing complete wetting would seem to be an important stage in the understanding of terraced wetting. Atomistic models are able to account for the details of the fluid-surface registration necessary for diffusive spreading. However, their use severely limits the system sizes which can be studied. Although several simulation studies have explored interactions of 8CB liquid crystals with crystalline substrates [17–20], the work presented here uses atomistic molecular dynamics simulations to examine liquid-crystal molecules spreading on surfaces.

In this paper we present simulation results for the spreading of an atomistically detailed fluid of liquid-crystal molecules on the (001) crystal plane of a generic face centered cubic (fcc) lattice. We employ a model 8CB liquid crystal molecule, which has been described in detail elsewhere [1]. The model 8CB molecule is derived from real 8CB, but uses a united-atom representation to eliminate hydrogen atoms, and possesses no electrostatic interactions. These simplifications were made in order to satisfy a need for computational efficiency, without sacrificing too much of the atomistic detail. It is inevitable, therefore, that this model will fail to provide detailed agreement with the experimental work on 8CB. For example, it cannot reproduce the phase transition temperatures of 8CB quantitatively (see Sec. II below), and does not possess the specific interactions responsible for the complex layering observed in the spreading of real 8CB systems [9]. However, the model 8CB molecule is useful for demonstrating generic liquid crystalline behavior, providing a convenient intermediate level of complexity between the single-site Gay-Berne models, and the fully atomistic or "all-atom" potentials that are used by some workers.

We begin with simulations of spherical droplets of model 8CB molecules in coexistence with their vapor, to analyze the nature of the phases present for a near spherical droplet. We then describe simulations of these droplets spreading on the fcc surface, for systems containing 595 and 1953 molecules, at temperatures of 350 and 425 K, on surfaces with various surface energies. For the spreading systems we focus on the radial dynamics and on the structure of the spreading monolayers. We also present the dynamics of the fluid-surface contact angle and internal mass flow fields.

II. METHODS

Molecular dynamics (MD) simulations were performed on droplets of model 8CB molecules, both in isolation and in contact with a crystalline substrate.

The model 8CB molecule has been discussed previously [1,19,21] and consists of a *united-atom* representation of 4-*n*-octyl,4′-cyanobiphenyl (8CB), in which the hydrogen atoms are subsumed into the adjacent carbon atoms and electrostatic interactions are ignored. The molecule possesses 22 distinct interaction sites which may be identified with the vertices and the cyano group in the standard stick representation of the molecule

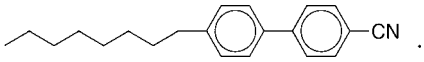

The potential energy expression employed consists of harmonic bond-length and bond-angle terms, a cosine expansion for bond torsions and a Lennard-Jones term for approximating the van der Waals interactions. The force field parameters were taken from the Amber force field [22] and from the work of Cross and Fung [23]. The parameters for the dihedral angle between the two phenyl rings were chosen to produce a twist of about 30° between their planes. A complete list of parameters has been given elsewhere [1].

The effect of electrostatic interactions on molecular packing can be important but usually modifies rather than dominates the behavior [24]. For our purposes, neglecting electrostatics greatly reduces computation times; the implementation of long range forces is particularly expensive in simulation work, increasing computation times by an order of magnitude. The molecular model was thus chosen for maximal computational efficiency while providing near-atomic detail. It yields generic liquid-crystalline behavior but, as a consequence of the lack of electrostatic interactions, fails to reproduce the phase behavior of the real 8CB system. For example, real 8CB has the following sequence of phases [25]:

$$\text{crystal} \xrightarrow{294.5\ \text{K}} \text{smectic } A_d \xrightarrow{306.5\ \text{K}} \text{nematic} \xrightarrow{313.5\ \text{K}} \text{isotropic},$$

where the smectic-A_d phase has an interdigitated bilayer structure, caused by antiparallel stacking of the polar 8CB molecules, whereas the model 8CB system has the following approximate simulated phase sequence [1]:

$$\text{smectic } A \xrightarrow{400\ \text{K}} \text{nematic} \xrightarrow{425\ \text{K}} \text{isotropic}.$$

The surface used in the spreading simulations is the (001) plane of a generic face centered cubic (fcc) solid. Each atom of the solid is connected to its twelve nearest neighbors by harmonic springs, of stiffness k_{ss}. k_{ss} is set equal to $\langle k_{ff} \rangle$, the mean bond stiffness averaged over all bonded atom pairs in the fluid. The equilibrium bond length d_{ss} is set equal to the average minimum energy separation between nonbonded fluid atoms, i.e., $d_{ss}=2^{1/6}\langle \sigma_{ff} \rangle$, where $\langle \sigma_{ff} \rangle$ is the average Lennard-Jones range parameter between the fluid atoms. The lattice constant a_0 is then set so that the nearest neighbor separation in the [110] direction is equal to d_{ss}, i.e., $a_0 = \sqrt{2} d_{ss}$. Choosing the lattice parameter for the surface in this way gives $a_0 \sim 5.9$ Å. The mass of the surface atoms is chosen to be comparable to the atomic masses of the fluid atoms, so that the time scales of the restoring forces in the solid and fluid are similar. In this way, the integration of the equations of motion remains efficient in the spreading system without the need for multiple time scales. The surface consists of

TABLE I. The parameters used to represent the generic fcc crystal surface, and its interactions with the fluid.

Parameter	Value
Atomic mass	20.0 g mol^{-1}
k_{ss}	3250.0 kJ mol^{-2} $Å^2$
d_{ss}	4.1557 Å
ε_{ave}	0.5270 kJ mol^{-1}
ε_{fs}	1.0 – 5.0
σ_{fs}	3.7025 Å

three layers of atoms. The atoms in the first and second layers are free to move in any direction, while those of the bottom layer are fixed in place. The parameters defining the surface are summarized in Table I.

The interaction between the surface and fluid atoms is of a Lennard-Jones form adding an additional term to the system potential

$$U_i = \sum_{j=1}^{n_{\text{surface}}} 4\varepsilon_{fs}\varepsilon_{ave}\left[\left(\frac{\sigma_{fs}}{r_{ij}}\right)^{12} - \left(\frac{\sigma_{fs}}{r_{ij}}\right)^{6}\right], \quad (1)$$

where i stands for a fluid atom, and the sum is over all atoms of the surface. The fluid-surface range parameter σ_{fs} was chosen such that $\sigma_{fs}^2 = \langle \sigma_{ff}^2 \rangle$. The strength of the fluid-surface interaction is conveniently expressed as the geometric average of the fluid-fluid values ε_{ave} (see Table I). However, in the simulations presented below, this value is scaled by ε_{fs}, which is a controlling parameter whose value determines the type of wetting that will occur. Therefore, in what follows, it is convenient to quote ε_{fs} as a dimensionless scaling factor for the average fluid-surface interaction energy.

Liquid droplets in stable coexistence with the vapor phase were simulated at constant volume, using the Nosé-Hoover implementation of the canonical NVT ensemble [26,27]. In all cases a collection of molecules at liquid densities was placed at the center of an enlarged simulation box and equilibrated for periods of up to 8 ns. Initial simulations consisted of 595 molecules (13 090 atoms) at 350 and 425 K corresponding to the smectic A and isotropic phases of the bulk system [1]. These simulations were equilibrated for 8 and 4 ns, respectively. Subsequently, larger systems of 1953 molecules (42 966 atoms) were equilibrated at the same temperatures. The equilibration of the larger systems was encouraged by basing their initial configurations on the equilibrated structure of the smaller systems. Thus at 350 K, the initial configuration of the large system was a spherical droplet with radial molecular orientations, while at 425 K the initial packing of the molecules was chosen to be isotropic. As a consequence, it was only necessary to equilibrate these larger systems for 2 ns.

Equilibrated droplets were positioned above the surface so that the bottommost atom of the droplet was at the distance of minimum potential energy from the surface, i.e., $z = 2^{1/6}\sigma_{fs} = 4.16$ Å. The total momentum of the fluid system was then rescaled to zero. MD simulations were performed on the fluid-surface system using the Berendsen NVT ensemble [28]. Thermostatting, through uniform velocity scaling, was applied only to the surface atoms and not the fluid atoms. In this way no artificial forces were applied to the fluid particles such as uniform momentum rescaling, which would be inappropriate in such an inhomogeneous system. Thus, thermostatting of the fluid particles was achieved purely through their thermal equilibrium with the surface atoms. This mechanism corresponds closely to that of the real system. In all simulations, a cutoff radius of 8.0 Å was used for the nonbonded potential and the simulation time step was 2 fs. This time step produced efficient momentum exchange between the surface and fluid atoms ensuring that the fluid remained in thermal equilibrium with the surface at all times. The value used is larger than normal for atomistic simulations, but is made possible through the use of united atoms and the consequent lack of high frequency C-H vibrations. The lateral size of the simulation box, i.e., in the plane of the surface, was chosen so that the spreading droplet did not come close to the box edge in the time scale of the simulation. For the 595 molecule simulations the lateral dimensions were ≈400 Å, while for the 1953 molecule simulations they were ≈700 Å. Periodic boundaries were not used.

Molecular dynamics simulations were carried out using the DL_POLY_2 open source MD code [29]. The standard DL_POLY_2 distribution was modified in order to perform running analyses of intramolecular and intermolecular properties of the system. The existing implementation of the Berendsen NVT ensemble was modified to rescale the momenta of the surface atoms only. Small simulations were used to establish the wetting conditions for the model, i.e., the values of ε_{fs} necessary for partial and total wetting. Certain key simulations were then repeated with the larger systems.

III. RESULTS

A. Establishing the conditions for wetting

1. Simulations of model 8CB droplets

The behavior of isolated model 8CB droplets was considered in a preliminary communication [21] and will be treated only briefly here. Droplets of model 8CB molecules in coexistence with their vapor were equilibrated at 350 and 425 K, prior to being lowered onto the (001) surface of an fcc substrate. The temperatures chosen correspond to the smectic A and isotropic phases, respectively, of the bulk systems [1]. Although we are principally interested in wetting behavior, the configurations of the isolated droplets are of interest in their own right and offer insight into the phase structure of the liquid-crystal fluid in the presence of a liquid-vapor interface and confined to a near spherical volume. In each simulation, a near spherical droplet was formed after about 50 ps, as might be expected since that shape minimizes the area of the liquid-vapor interface and presumably also the free energy, although this is not guaranteed in an anisotropic system.

The systems at 350 K exhibit a predominantly radial alignment of molecular axes, which might be expected since homeotropic anchoring is strongly favored at the liquid-

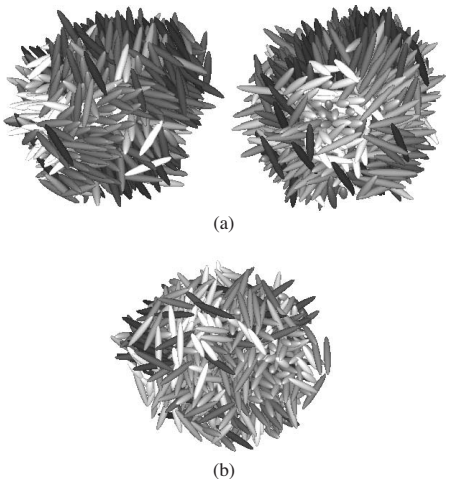

FIG. 1. (a) Two snapshots of a droplet of 595 model 8CB molecules, taken 0.5 ns apart after equilibrating for 8 ns at 350 K. (b) The same system after equilibrating at 425 K. To aid visibility, each molecule has been replaced by an ellipsoid aligned with the molecular long axis. The ellipsoids are shaded according to their orientations within the simulation box; dark gray corresponds to a large x component, light gray corresponds to a large y component, and midgray corresponds to a large z component of the molecular director. N.B. The images show the central c. 25 % of the simulation box in each case.

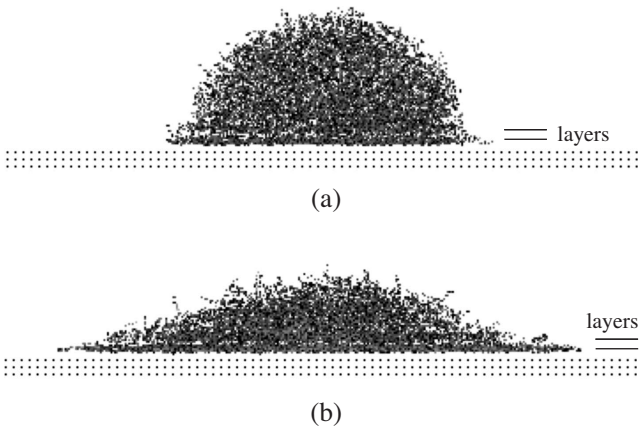

FIG. 2. Snapshots of liquid-crystal droplets during spreading, consisting of 595 molecules after 4 ns at 350 K: (a) sessile equilibrium structure during partial wetting of the solid surface $\varepsilon_{fs}=2.0$; (b) continuing spreading during complete wetting, with $\varepsilon_{fs}=2.5$. An atomistic representation is used, with each atom drawn as a dot.

vapor interface for this model [30] and has been observed in real nCB systems using ellipsometry [31]. There is a tension, however, between the preferred radial alignment and the symmetry of the smectic A phase, which requires the molecules to arrange into layers. In the simulations, we are able to observe the formation of layers, but there is a constant shifting of the layer normal relative to the droplet, combined with constantly changing deviations from the spherical form. The details of the internal structure in the simulation change repeatedly over time scales of about 1 ns [see Fig. 1(a)], indicative of the inherent instability in the equilibrium configuration. Similar shape changes have also been observed experimentally. For example, studies of 8CB droplets in the smectic-A_d phase show evidence of stratification, with the surface of the droplet forming a system of terraces [32]. At 425 K, the droplet appears isotropic, and as expected retains a spherical shape [Fig. 1(b)].

2. Terraced wetting of liquid-crystal droplets

The small, 595 molecule, liquid-crystal droplets were used to explore the dependence of wetting behavior on the value of the fluid-surface interaction parameter ε_{fs}. The equilibrated 350 and 425 K systems were placed in contact with (001) fcc crystal surfaces with different values of ε_{fs}, and allowed to spread under the influence of that interaction. The wetting characteristics appear to depend sensitively on the value of ε_{fs}. For example, at 350 K and $\varepsilon_{fs}=2.0$, we obtain partial wetting and the profile of the droplet is essentially static as shown in Fig. 2(a). On the other hand, the same system with $\varepsilon_{fs}=2.5$ exhibits continuous spreading for the duration of the simulation [Fig. 2(b)].

The onset of complete wetting was observed to occur at 350 K for a value of ε_{fs} between 2.4 and 2.5, while at 425 K it occurred for ε_{fs} between 2.0 and 2.1. At each temperature, lower values of ε_{fs} promoted sessile structures, i.e., partial wetting. The behavior of the larger, 1953 molecule droplets was consistent with that of the smaller systems. In the completely wetting systems, distinct molecular monolayers are visible in snapshots of the spreading fluid (see Fig. 3). These precursor films, which grow out in advance of the main spreading droplet, are characteristic of "terraced wetting." In the figure, a second terrace is also visible. The precursor films observed in the simulations consist of a single monolayer of molecules in agreement with experimental studies of complete wetting systems [3,4].

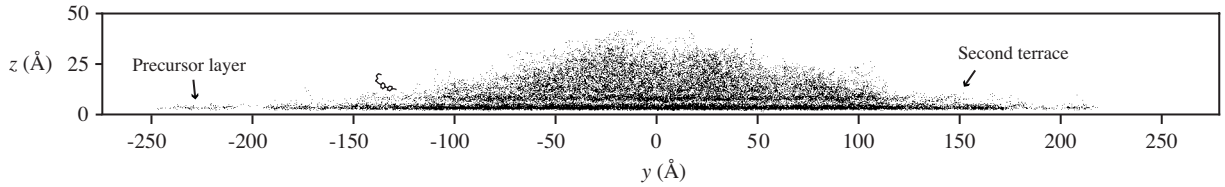

FIG. 3. The profile of a spreading droplet of 1953 molecules undergoing terraced wetting at 425 K, with $\varepsilon_{fs}=2.5$. The snapshot was taken after 2.5 ns of spreading. An atomistic representation is used, and the precursor film is indicated. A single liquid-crystal molecule is outlined to provide an indication of scale.

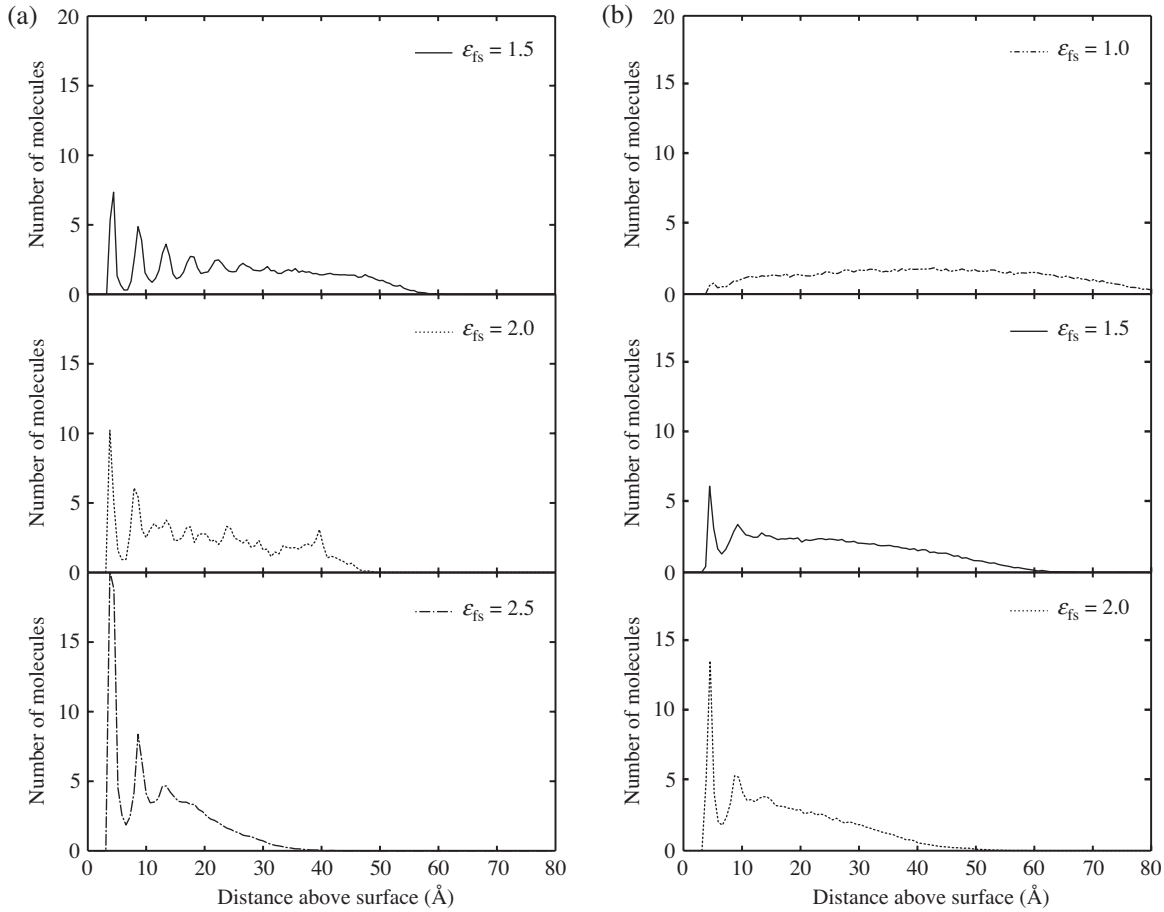

FIG. 4. The number density of molecules as a function of distance from the surface for systems at (a) 350 K and (b) 425 K for different values of the surface-fluid interaction ε_{fs}. The profiles are short time averages of 100 ps, after approximately 4 ns of spreading.

B. Droplet structure during wetting

1. Molecular layering

Whether the wetting is partial or complete, we observe layering parallel to the surface similar to that seen in simple fluids, as indicated in Fig. 2. This is shown quantitatively in Fig. 4, which shows profiles of the number density of liquid-crystal molecules normal to the surface, for droplets on surfaces with various values of ε_{fs}, at 350 and 425 K. The layering is quite distinct both for the sessile droplets partially wetting the surface and for systems nearing complete wetting. The layering appears most pronounced for the lower temperature system, for low values of ε_{fs}. For example, at 350 K and $\varepsilon_{fs}=1.5$ we observe at least seven clear layers, which is a consequence of the tendency to form layers being enhanced by the liquid-crystalline packing of the molecules in the droplet. As ε_{fs} is increased, the upper layers become disrupted, and at the transition to complete wetting, i.e., when ε_{fs} is slightly less than 2.5, only three layers remain visible with, however, the first molecular layer considerably more pronounced. The shape of the distribution is without doubt a consequence of the fact that the molecules are spreading rapidly across the substrate, thus limiting the z extent of the model. At the higher temperature 425 K, with $\varepsilon_{fs}=1$ the droplet is barely wetting the surface, and the system is in its isotropic phase, so that there is only a minimal indication of layering. As ε_{fs} increases, we observe the formation of layers close to the substrate. However, unlike the 350 K models, there is no driving force from the liquid crystalline phase to enhance the layering; the layering is solely a result of the surface interaction. Finally, at $\varepsilon_{fs}=2.0$, i.e., very close to the transition to complete wetting, the appearance of the distribution at 425 K is very similar to the equivalent one at 350 K. In all cases where layering occurs, the spacing between the molecular monolayers is approximately 4.5 Å, and shows little variation with temperature.

2. Equilibrium structure during partial wetting

As explained above, for values of ε_{fs} below a critical value we observe *partial* wetting of the surfaces and the formation of *sessile* equilibrium structures. The equilibrium configurations reflect properties of the bulk fluid and the fluid-surface interaction as well as anchoring conditions at the fluid-vapor and fluid-surface boundaries.

Figure 5 shows coarse-grained representations of the equilibrium structure of large droplets (1953 molecules) at 350 K with $\varepsilon_{fs}=2.0$, i.e., slightly below the value required for complete wetting. After equilibrating for 4 ns, the droplet adopts the static splayed "hedgehog" structure seen clearly in Fig. 5(a). This appears to be the minimum free-energy configuration, and is consistent with homeotropic alignment of

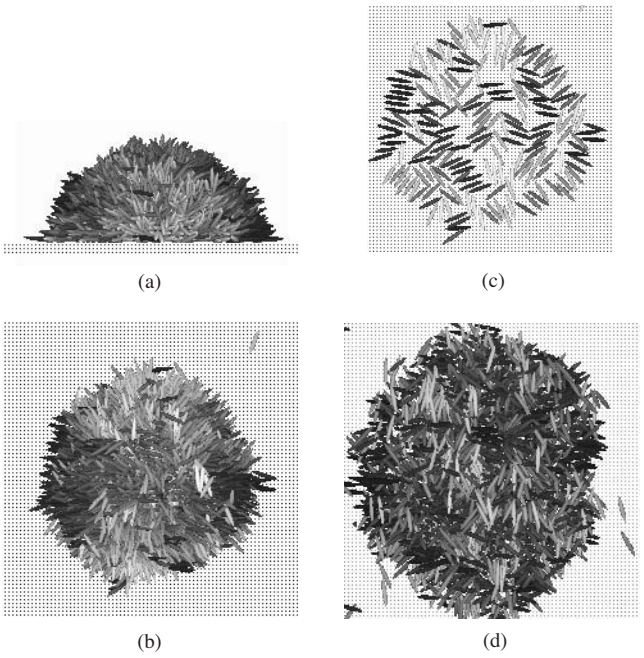

FIG. 5. The equilibrium structure of partially wetting droplets at 350 K with $\varepsilon_{fs}=2.0$: (a) side view, indicating homeotropic and planar anchoring at the liquid-vapor and liquid-surface interfaces, respectively; (b) view normal to surface, revealing a radial director structure at the droplet edge; (c) snapshot of molecules in the surface layer only, for the same system as (a) and (b); (d) the same system at 425 K. All parts are drawn to the same scale. The shading of the ellipsoids is the same as in Fig. 1. N.B. The images show the central ≈25% of the simulation box in each case.

molecules at the liquid-vapor interface and planar alignment of molecules at the surface.

The view normal to the surface [Fig. 5(b)] reveals a director structure which is predominantly radial. The circular symmetry is perturbed, however, by the formation of unsplayed rows of molecules at the edges of the droplet. This is consistent with the tendency to form localized smectic ordering which was observed in isolated droplets at this temperature. If we examine the arrangement of molecules in the adsorbed layer only [Fig. 5(c)] we see that the splayed director structure apparent at the surface does not persist all the way to the center of the droplet, where it would form a point defect. Rather we see small regions of localized order surrounded by the radially aligned ring of molecules on the perimeter. The molecular length sets a minimum length scale for the system. This means that close to the center of the wet region, we can infer that the free energy cost associated with director splay becomes too large and the formation of a central point defect is not favored.

In contrast to the droplet at 350 K, the "isotropic" sessile droplet at 425 K shows very little ordering at the liquid-vapor interface [see Fig. 5(d)]. There is still, however, an indication that the substrate is influencing the overall shape of the droplet, as the radial symmetry is far from perfect.

3. Structure of adsorbed monolayers during spreading

In this work we are particularly interested in the detailed structure of the spreading monolayer and the macroscopic

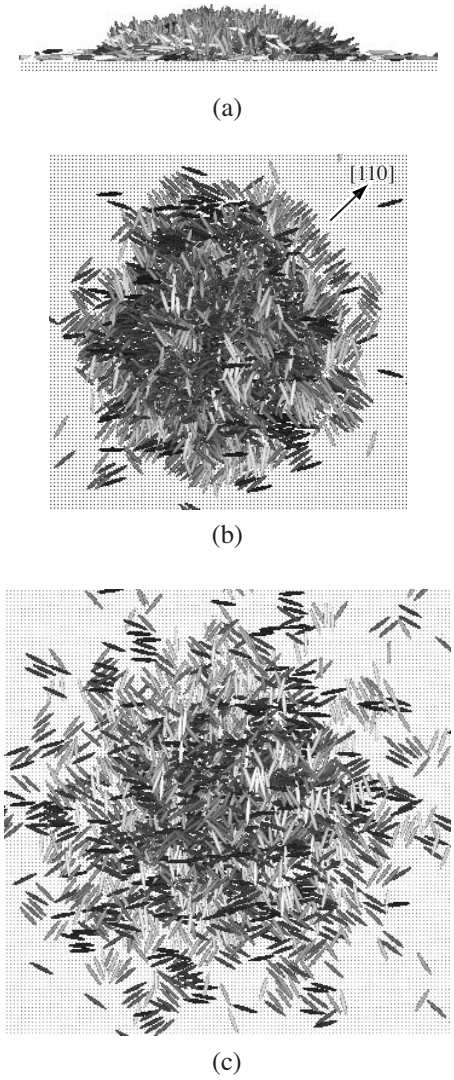

FIG. 6. Coarse-grained snapshots of a 1953 molecule system undergoing complete wetting ($\varepsilon_{fs}=2.5$). (a) Side view of the system at 350 K. Homeotropic alignment is clearly visible at the free liquid-vapor interface. (b) The same system as (a) viewed from above. The monolayer tends to adopt a diamond shape. (c) The same system at 425 K. The spreading droplet has a higher degree of radial symmetry than at 350 K. All images created after spreading for 2.4 ns. N.B. The images show the central ≈25% of the simulation box in each case.

fluid reservoir. Figure 6(a) shows a side view of the 350 K system undergoing complete wetting. The homeotropic alignment at the free liquid-vapor interface, which was observed in the isolated droplet at 350 K (see above), is again present during spreading. Planar alignment of molecules wetting the surface is observed in the emerging precursor film.

Figure 6(b) shows coarse-grained snapshots of the spreading of the 350 K droplet viewed normal to the surface. The long axes of molecules in the wetting layer clearly lie parallel to the surface. Of particular interest is the shape of the wetting film. As noted previously [21], the spreading droplet appears not to be completely radially symmetric, instead forming a diamond shaped monolayer as it spreads. The

edges of the diamond lie perpendicular to the [110] directions, and are characterized by the appearance of two-dimensional close-packed smectic layers in the wetting film. This behavior appears to be a consequence of the tendency for the long axes of molecules wetting the surface to lie along grooves in the [110] directions of the (001) surface planes of the fcc lattice. It is worth emphasizing that the appearance of Fig. 6(b) is not a consequence of boundary effects in the simulation box; only the central ≈25% of the box is shown, and the box extends for several molecular lengths beyond the edge of the spreading droplet.

The appearance of the spreading droplet at 425 K [Fig. 6(c)] is in stark contrast to the 350 K system. Apart from some localized orientational ordering, the precursor film in this case appears to have near-circular symmetry, although the growing edge is poorly defined and disordered. Most notably, the close-packed two-dimensional layering in the plane of the substrate is lost. There is also a pronounced difference between Fig. 6(c) and the partial wetting system at the same temperature [Fig. 5(d)], the latter possessing a clearly defined boundary, and less perfect circular symmetry.

The diamond-shaped precursor layer in the 350 K system appears to result from three factors: (1) residual orientational ordering between molecules consistent with the bulk smectic phase structure, (2) orientational anchoring of molecules along grooves in the (001) surface, and (3) radial director alignment at the macroscopic droplet edge. The third point, a strong favoring of radial alignment at the macroscopic droplet edge was noted in the simulations of partial wetting droplets (see above). Radial alignment on the crystal substrate may be regarded as a two-dimensional analog of the homeotropic alignment commonly observed at free surfaces in these systems. It is reasonable to assume that this tendency is also present during complete wetting.

Thus, for the 350 K system with $\varepsilon_{fs}=2.5$ we observe orientational ordering between molecules in the two-dimensional surface layer which is consistent with the orientational ordering observed in the bulk at the same temperature. In addition we observe strong orientational coupling to the surface. This represents a significant observation specific to liquid crystal systems that translational degrees of freedom are dominated by diffusive motion, while under certain conditions, orientational anchoring with the surface and weak liquidlike orientational order remain. For the system at 425 K in equilibrium with the bulk isotropic state point we see some localized orientational ordering in the spreading monolayer, which is probably due to the strong orientational anchoring effect of the substrate.

4. Surface registration

As indicated above, there is a tendency for the liquid-crystal molecules in a spreading droplet to align with the [110] directions in the substrate. For the (001) plane of the fcc surface the [110] directions correspond to the loci of local minima in the surface potential, forming distinct "grooves" in the surface. For anisotropic liquid crystal molecules the potential energy is best minimized when the molecules run along these grooves. In fact, a close examination of Fig. 5(c) suggests that there is also some preference for orientations close to the [100] directions of the substrate. However, increasing ε_{fs} to 2.5, i.e., switching from partial to complete wetting, has the effect of polarizing the system into the [110] orientations, as exemplified by Fig. 7 which shows the wetting layer directly beneath the fluid reservoir at 350 K. A similar surface induced orientation has been observed in previous simulations of liquid crystal molecules on a range of different crystalline and corrugated surfaces [19,20].

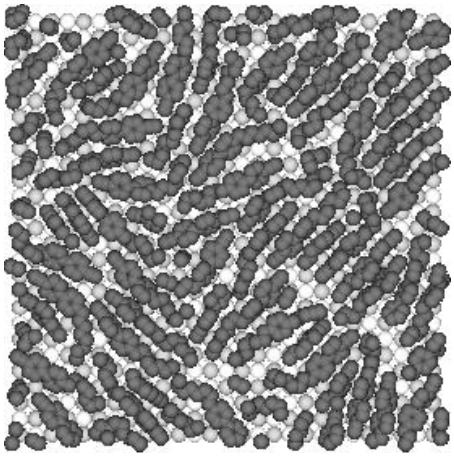

FIG. 7. Closeup of molecules adsorbed on the surface directly beneath the fluid reservoir of the droplet ($T=350$ K, $\varepsilon_{fs}=2.5$). Atoms are attracted to the minima in the surface potential causing the molecules to lie along the "grooves" in the [110] (diagonal) directions.

5. Molecular shape of adsorbed molecules

In a previous paper [1] it was noted that, as the bulk model 8CB liquid crystal is cooled through the order-disorder transition, the molecular shape becomes more biaxial. In the present case, we examine the change in shape as the molecule becomes adsorbed onto the substrate. The molecular shape is characterized by the principal components of the moment of inertia tensor. If L_1, L_2, and L_3 are the eigenvalues of the moment of inertia tensor then the shape of a molecule can be taken as the dimensions of an *equivalent inertia ellipsoid* with principal axes $(A,B,C)=(L_1^{-1/2},L_2^{-1/2},L_3^{-1/2})$ [33]. If we order the eigenvalues such that $A>B>C$, A/C represents the aspect ratio of the molecule and B/C indicates the departure from uniaxial symmetry, i.e., the biaxiality.

Table II shows the average aspect ratio and biaxiality for the molecules in the wetting layer compared with molecules of the fluid reservoir, for systems with $\varepsilon_{fs}=2.5$. It can be seen that the molecules of the wetting layer are slightly more biaxial than those in the fluid reservoir at both 350 and 425 K, and also have a slightly higher aspect ratio. Similar changes were observed for $\varepsilon_{fs}=2.0$ (not shown). Although the differences shown in the table are small, nevertheless they are statistically significant.

Averaging the moment of inertia tensor components over the molecules of the adsorbed layer prior to diagonalization, gives the average eigenvalues and eigenvectors throughout

TABLE II. Aspect ratio (A/C) and biaxiality (B/C) for liquid-crystal molecules in the fluid and in the wetting layer of droplets on a surface with $\varepsilon_{fs}=2.5$. Also included are values for the bulk phase taken from Ref. [1].

	$T=350$ K		$T=425$ K	
	A/C	B/C	A/C	B/C
Fluid	3.225(1)	1.0304(2)	3.213(1)	1.0292(2)
Surface	3.233(2)	1.0325(4)	3.220(2)	1.0307(4)
Bulk	3.231(1)	1.0315(1)	3.218(1)	1.0301(1)

the adsorbed layer. The eigenvector of the largest eigenvalue, corresponding to the axis of the smaller lateral dimension of the average equivalent inertia ellipsoid is parallel to the z axis in all cases, i.e., exactly normal to the surface. This is the direction of the imposed biaxiality and suggests that the molecules are flattened in the plane of the surface.

Interestingly, the biaxiality and aspect ratios obtained in simulations of the bulk phase are intermediate between the fluid and surface values shown here. This is probably a consequence of the fact that the fluid phase of the droplet is less well ordered than the bulk phase, which is, in turn, a result of the boundary conditions imposed by the substrate and the free surface of the droplet.

C. Spreading dynamics

1. Rates of spreading

The spreading dynamics of the monolayer closest to the surface were analyzed for droplets undergoing complete wetting. Figure 8(a) shows the number of particles in the monolayer closest to the surface as a function of time. In all cases the limit of the first monolayer is taken as the minimum in the corresponding density profile normal to the surface (see Fig. 4). After an initial period of ≈ 1 ns, corresponding to the settling of the droplet onto the solid surface, we see that the increase in the number of molecules in the adsorbed layer N rises approximately linearly with time for $\varepsilon_{fs}=2.5$, but levels off to a constant value for a sessile droplet with $\varepsilon_{fs}=2.0$. The spreading rate appears substantially faster at 425 K than at 350 K for the same value of ε_{fs}. Assuming a uniform density in this layer and circular symmetry, it follows that $N(t) \propto R(t)^2$, where $R(t)$ is the precursor layer radius. Thus linear growth of N with time is consistent with radial spreading as the square root of time, $R(t) \propto \sqrt{t}$, in agreement with experimental observations [3].

A more quantitative estimate of the growth rate was obtained by measuring the radius of the droplet directly during the simulation. The method adopted determined the droplet radius from the radius of gyration of the lowest adsorbed layer of molecules in the plane of the substrate. The resultant spreading dynamics are shown for the two key state points in Fig. 8(b), which shows logarithmic plots of the increase in radius over the initial value $R(t)-R(0)$ as a function of time. The solid lines are lines of best fit with gradients of 0.5, fitted to the region $R(t)-R(0) \gtrsim 30$ Å. Similar spreading behavior is observed at temperatures corresponding to both isotropic and smectic bulk phases. From Fig. 8(b) we determine a diffusion constant for spreading at 350 K as 0.92 Å^2 ps^{-1}, compared to 5.25 Å^2 ps^{-1} at 425 K. It should be noted that the deviations from the $\sqrt{t}$ law observed at the shorter time scales in Fig. 8(b) arise due to a combination of poor counting statistics and the fact that the droplet has not made complete contact with the substrate in this part of the plots.

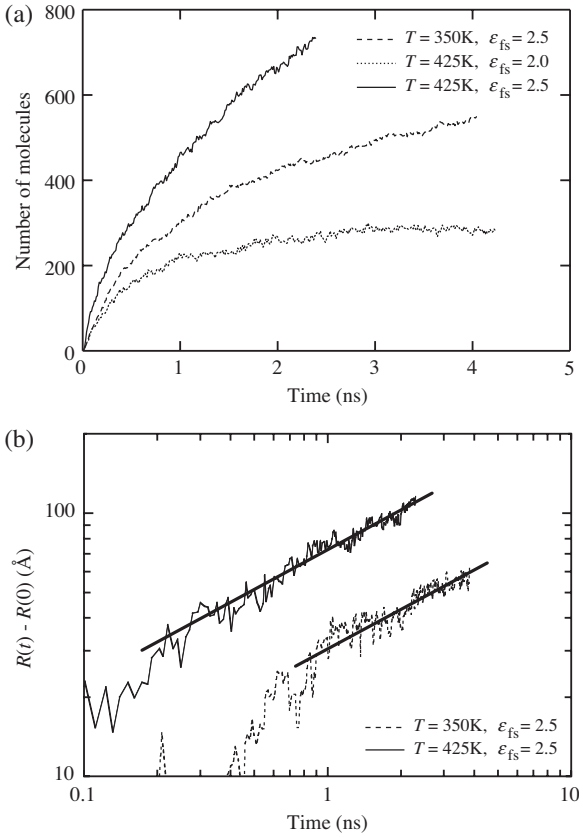

FIG. 8. (a) The number of particles in the precursor layer versus time. A region of approximately linear growth corresponds to radial spreading with $R(t) \propto \sqrt{t}$. (b) Radial growth of the wetting monolayer over time, determined from the radius of gyration. The fit lines have gradients of 0.5.

It has been observed experimentally that, during complete wetting, the precursor film spreads like a two-dimensional gas with diffusion taking over from liquid cohesion. It follows that there is no molecular anchoring at the surface in simple fluids [3]. From the low density of the precursor film in our simulations and the radial spreading dynamics $R(t) \propto \sqrt{t}$ observed we conclude that our wetting film also resembles a two-dimensional gas. We should expect no strong molecular anchoring of the *centers of mass* of the molecules.

In order to investigate the symmetry of spreading droplets in a more quantitative way, we divided the surface into eight radial segments of equal angular width, $\pi/4$ radians, centered on the four [100] and four [110] directions in the surface. Figure 9 shows the growth with time of the average radii of the four [100] segments and of the four [110] segments, for the two key complete wetting systems at 350 and 425 K. Although the statistics for the calculation of the segment by segment radius are relatively poor, there appears to

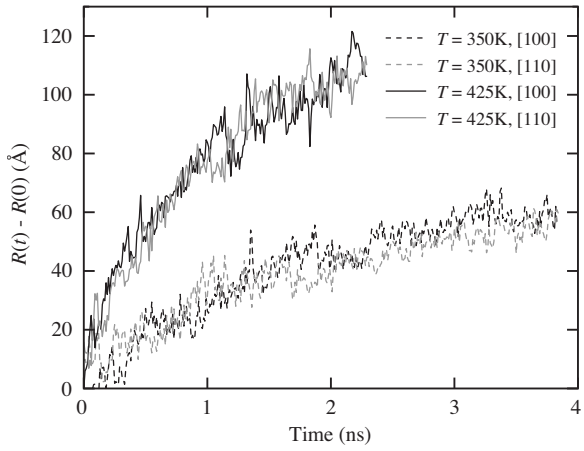

FIG. 9. Growth of the precursor layer radius along the [100] directions and along the [110] directions, in completely wetting systems.

be no systematic difference between the growth rates of the [100] and [110] radii for either the 350 K or the 425 K system.

2. Effect of growth rate on precursor shape

It was suggested above, that the diamond-shaped precursor layer in the 350 K system results from a combination of residual liquid-crystalline ordering from the bulk smectic phase, orientational anchoring along grooves in the crystal surface, and radial director alignment, which is the two-dimensional equivalent of homeotropic alignment, at the macroscopic droplet edge. Looking at the effect of the liquid-solid coupling strength on the structure of the spreading film provides further insight into these mechanisms. In much the same way as in regular crystal nucleation, the growth rate of the precursor film appears to be a critical factor. Figure 10(a) shows a snapshot of a system of 595 molecules with $\varepsilon_{fs}=3.0$. Here we do not see the regular homeotropic alignment at the edges of the spreading film, which is probably a consequence of the smaller system size and the higher growth rate of the film in this system. As a result, a diamond-shaped wetting monolayer is not formed. However, the alignment with the grooves in the [110] directions is still manifest. The same system with $\varepsilon_{fs}=5.0$ is shown in Fig. 10(b). Here the growth rate is higher still and, again, the diamond-shaped wetting monolayer is not formed. In addition, the weak smecticlike liquid cohesion appears to be overcome by the very strong liquid-solid coupling and the presence of two-dimensional smecticlike layers is not pronounced. It is also worth noting that the growth rate is higher in systems at 425 K than at 350 K (Fig. 8) and that this may account, in part, for the difference in morphology between Figs. 6(b) and 6(c).

3. Contact angle dynamics

The contact angle at the point of intersection of surface, liquid, and vapor is a useful dynamical property in many theories of wetting, reflecting the surface tensions of the liquid-vapor, liquid-solid, and solid-vapor interfaces.

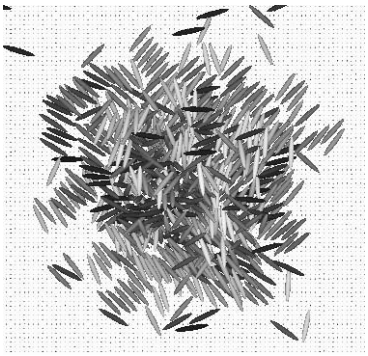

(a)

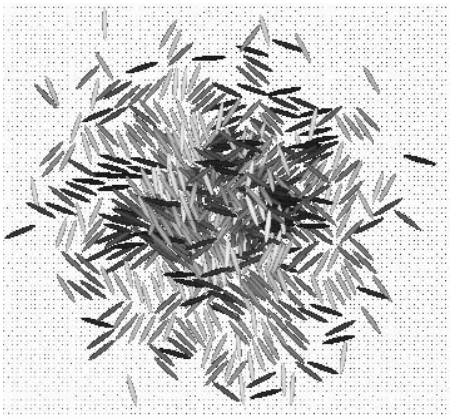

(b)

FIG. 10. 595 molecule droplets spreading at 350 K with (a) $\varepsilon_{fs}=3.0$ and (b) $\varepsilon_{fs}=5.0$.

The variation in contact angle with time was measured for cases of partial and complete wetting at different temperatures. The procedure for obtaining the contact angle at each time involved straight line fits to the foot of the droplet profile at four points around the circumference corresponding to the principal [100] axes of the surface. The average angle these lines made with the surface was then taken as the contact angle.

Figure 11 shows plots of the variation in contact angle during spreading. The broad qualitative features of the decay of the contact angle with time are in excellent agreement with contact angle dynamics measured in recent spreading experiments [7,34]. They also agree well with simulations of spreading chain molecules [6]. Differences in time scale between simulation and experiment may be explained by the differences in droplet volume considered. A contact angle of 180° corresponds to a perfect sphere sitting on the surface, while a zero contact angle corresponds to complete wetting. In each case the contact angle approaches a fixed value at large times. For partial wetting this angle reflects the competing surface tensions at the liquid-vapor and liquid-solid interfaces [8]. For complete wetting the contact angle decays to zero.

4. Mass transfer within the droplet

The average velocity field of the molecular centers of mass throughout the fluid droplet has been measured at dif-

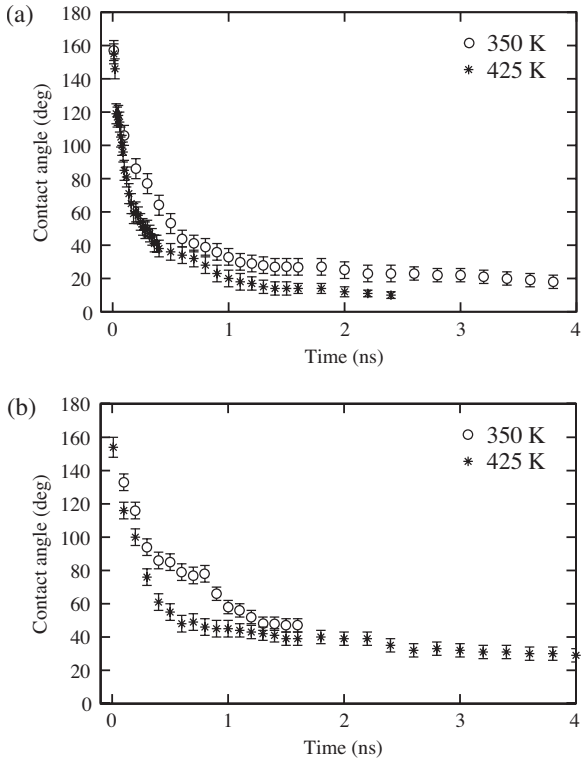

FIG. 11. The variation in contact angle of a spreading droplet with time in cases of (a) complete wetting (ε_{fs}=2.5) and (b) partial wetting (ε_{fs}=2.0).

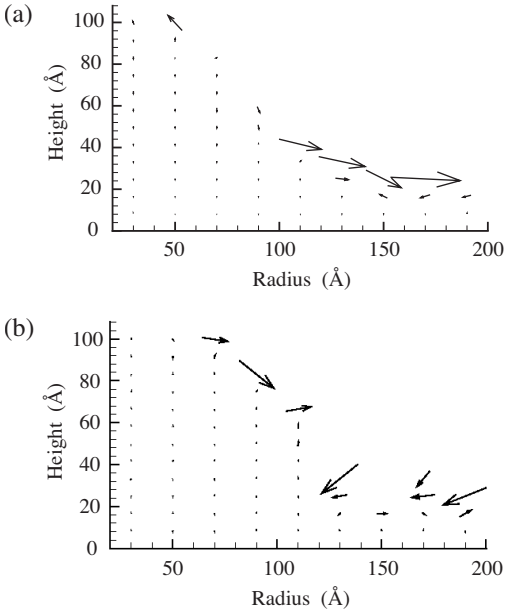

FIG. 12. Velocity profiles of droplets at 425 K: (a) the terraced wetting regime during the initial preterracing spreading period (ε_{fs}=2.5, t=0–1 ns); (b) during the latter stages of partial wetting (ε_{fs}=2.0, t=2–3 ns).

ferent stages of the simulations. The velocity field is indicative of the dynamics of mass transfer within the spreading droplet. In particular, we are interested in the mechanism by which the molecules move from the "reservoir" of the body of the droplet to the wetting precursor film.

Velocity fields in molecular simulation are notoriously noisy. In an effort to improve the statistics and reduce noise the vector field has been averaged over a 1 ns time period. The droplet is partitioned into cylindrical shells at radial intervals of 20 Å and intervals of 4.5 Å in the z direction, corresponding to the observed molecular layer spacing. Spatial averaging takes place over these cylindrical bins.

Figure 12(a) shows the velocity fields within a droplet at 425 K in the early stages of complete wetting (t=0–1 ns). The most notable feature is the strong velocity field at the edge of the droplet driving the rapidly emerging precursor film. The velocity fields are consistent with a mechanism where molecules migrate over the outer surface of the droplet on their way to the spreading precursor film, a mechanism proposed by de Gennes and Cazabat for the preterracing period of the spreading [5]. A small component in the $-z$ direction is apparent, closer to the center of the droplet, as the fluid reservoir slowly subsides.

The velocity fields in partially wetting systems have also been examined. Figure 12(b) shows velocity fields for the 425 K system for the 2–3 ns period. Here it appears that the fluid molecules are unable to penetrate into the precursor wetting layers, instead returning to the fluid reservoir at a higher level. Such behavior would again be in qualitative agreement with the theory of de Gennes and Cazabat [5] and has been observed previously in simulations of simple fluids [15].

IV. DISCUSSION

The results presented above have demonstrated the spreading of droplets of liquid-crystal molecules on crystalline surfaces at a microscopic level. Much of the behavior observed, for example, the formation of a precursor layer, the diffusive spreading mechanism and the mass transfer within the droplet, is common to simple liquids. However, there are some features of the spreading behavior that are dependent on the mesogenic nature of the molecules. In particular, we refer to the molecular orientation and layer formation within the spreading droplet, and, for lower spreading rates, the diamond shape of the precursor film [Fig. 6(b)].

This unusual spreading morphology is seen to be a consequence of an interplay between the mesogenic orientational ordering, strong fluid-substrate interactions that orient the molecules in the [110] directions in the surface plane and boundary conditions that favor homeotropic orientation of the liquid crystal molecules at the surface of the droplet. Of these, it is the homeotropic boundary condition that appears to have the dominant effect. Strong homeotropic alignment is found at the liquid-vapor interface in spreading droplets at temperatures corresponding to smectic ordering in the bulk system. This observation agrees with recent simulations of *planar* liquid-vapor interfaces at similar temperatures [30], and also with experimental results [31].

An explanation for this preference may be given in terms of the relative sizes of the elastic constants in the system. It is well established for orientationally ordered liquid crystals that the bulk elastic constant is higher for bend deformations

than for splay. Homeotropic (radial) alignment at the surface of a sphere would represent a *splayed* director field while planar alignment would require a *bent* director field. Thus we would expect homeotropic anchoring at the liquid-vapor interface to be even stronger in the case of a spherical interfacial surface. This accounts for the highly ordered splayed 'hedgehog' configurations observed for sessile droplets at 350 K and $\varepsilon_{fs} \leq 2.0$.

In addition, it is possible that the presence of the liquid-vapor interface in the droplet system stabilizes the smectic-like phase due to the free energy penalty associated with "bend" deformations of the director field around the spherical surface. However, bulk simulations at the same temperature, with periodic boundary conditions, also predict a smectic-*A* phase [1], which gives us confidence that the smectic phase observed is not an artifact of the small system size and periodic boundary conditions. Ultimately, this question cannot be resolved without larger simulation sizes, which will be the subject of future work.

An abrupt transition was observed from partial wetting to complete wetting as the strength of the fluid-surface interaction was increased. This sensitive dependence on the energetics of the surface is in qualitative agreement with experimental observations of partial and complete wetting on high- and low-energy surfaces [4]. The higher temperature system was more inclined to complete wetting, requiring a lower value of ε_{fs} to induce wetting. To understand the crossover from partial to complete wetting we can imagine a number of competing influences within the system. Firstly, favoring the formation of a sessile, near-spherical droplet on the surface we have (1) the liquid cohesion of the drop due to the Lennard-Jones interaction, (2) the desire to minimize the surface free energy and form a sphere, and (3) the adoption of the preferred homeotropic anchoring at the liquid-vapor interface, which is not possible for planar aligned monolayers completely wetting the surface. Favoring complete wetting of the surface is (4) the attractive part of the surface-fluid interaction. The energy scale for the effect of gravity on the system is many orders of magnitude less than the Lennard-Jones interaction and should not be significant. Factors (1) and (4), the liquid cohesion versus the surface-fluid attraction, appear to be the key competing factors. It was noted that the higher temperature, 425 K, system required a lower value of ε_{fs} to induce wetting. This is consistent with a less dominant liquid cohesion at 425 K compared with the 350 K system.

The height of the spreading droplets is approximately the same as those observed experimentally, at around 50 Å. However, the lateral extent of the precursor film in the case of terraced wetting is many orders of magnitude smaller than for the droplets observed experimentally: just 200 Å compared with a few mm. The small size of the droplet in the simulation limits the reservoir of molecules available to the spreading foot. The rate of radial spreading, however, would not be expected to depend on the size of the system while sufficient molecules remain in the fluid reservoir, if the spreading is diffusive. Heslot *et al.* observe that spreading of the precursor film only starts to slow when just a few molecular layers remain of the fluid reservoir [3,4].

During spreading it was observed that the 350 K droplet maintained strong homeotropic anchoring at the liquid-vapor interface. The splay imposed on the director field in this case is less severe than for the spherical surface of the isolated droplet. The free energy cost associated with a splayed director field means that homeotropic alignment at the free liquid-vapor interface is stabilized by the droplet wetting the surface. Of course the planar aligned precursor film does not permit homeotropic alignment at the liquid-vapor interface at all and it is unclear exactly what the influence of the liquid-vapor interfacial anchoring on the wetting characteristics might be. A detailed comparison of the velocity fields for equivalent 350 and 425 K wetting systems (either partial or complete) should give insight into the role played by the interfacial anchoring. This has not been possible here, due to the large fluctuations inherent in such a small model. The contact angle might also be expected to be affected by the homeotropic alignment at the liquid-vapor interface. A more detailed study of both is required, involving larger system sizes, to make progress with these suggestions.

So far, all simulations have been performed on the same (001) fcc crystal surface, albeit with different values of ε_{fs}. It would be interesting to vary the lattice constant, or use different surfaces, in order to determine under what conditions the diffusive spreading dynamics break down and how the structure of the precursor film is affected by changing the width and spacing of the corrugation in the surface.

It is apparent that the spreading behavior of liquid-crystal droplets depends sensitively on the interactions between the liquid-crystal molecules and the substrate, and on the structures of both. In this respect, the atomistic model employed here has an advantage over the course-grained equivalents, allowing a much finer tuning of the energy terms. The flattening of the molecules onto the substrate, i.e., the biaxiality shown in Sec. III B 5, is another aspect of behavior that we could not expect to find in coarse-grained systems. However, it should be clear that the present model still represents only an intermediate step between coarse grained and fully atomistic simulations.

For example, and as noted in the Introduction, the real 8CB system exhibits rather different behavior from that described here. The main differences are (1) the spreading of both a monolayer and a trilayer of liquid-crystal molecules and (2) the fact that the molecules in the monolayer are tilted away from the substrate [9]. The trilayer is in fact a combination of monolayer and smectic bilayer. It would appear unlikely that the model 8CB system considered here would be able to reproduce this exact behavior, principally because of the lack of electrostatic interactions, which are likely to be responsible for stabilizing the bilayer, and promoting the tilt of the monolayer molecules. However, such behavior is specific to the *n*CB family of molecules, whereas the model system utilized here is designed to reproduce more generic types of behavior. In addition, it seems probable that much larger simulation sizes would be needed, before it would be feasible to successfully simulate a trilayer. Despite these limitations, the model presented here has proved very successful in developing an understanding of the molecular mechanisms of the spreading of liquid-crystal droplets.

Finally, it is worth commenting that the experimental time scales for complete wetting with a precursor foot of macroscopic dimensions are of the order of many hours. Such time

scales are inaccessible in simulation work. In fact, the wetting monolayer we observe in our simulations is only about twice the diameter of the fluid reservoir. However, despite this limitation, the simulations presented here still provide a useful insight into the nature of the precursor film, both in terms of its detailed structure, and the dynamics of its spreading.

V. CONCLUSIONS

Simulations of isolated droplets show regions of localized order consistent with the phase structure of the bulk system. Smectic order in these systems appears to be frustrated by the spherical symmetry of the droplet imposed by the surface tension and the tendency to assume a homeotropic (radial) alignment at the liquid-vapor interface.

With a relatively simple atomistic model we have simulated spreading of a droplet of liquid crystal on an atomically detailed surface. For suitable values of the surface-fluid interaction strength ε_{fs}, terraced wetting was observed exhibiting the characteristic layering and radial spreading dynamics ($\propto\sqrt{t}$), as observed in simple fluids. Measurements of the variation of the contact angle with time and of velocity fields within the spreading droplet are in broad qualitative agreement with experiment and previous simulations of simple fluids. The studies of mass flow within the droplets indicate that spreading occurs by molecules cascading over the top of the droplet to join the precursor layer.

In all cases it was observed that the molecules of the wetting layer were less uniaxial (i.e., "flatter") and more elongated than the molecules of the macroscopic fluid reservoir. Although the difference was small, it was, nevertheless, statistically significant.

Under certain conditions the shape of the precursor film was not radially symmetric. A diamond-shaped wetting monolayer was formed at 350 K, which is attributed to weak smecticlike liquid cohesion, orientational coupling of molecular directors along the [110] directions in the (001) fcc surface, a slow growth rate of the wetting monolayer, and a surface-fluid interaction just strong enough to produce complete wetting. Orientational anchoring with the surface occurred through the alignment of molecules along natural corrugations in the (001) surface.

For partial wetting droplets in equilibrium with the bulk smectic state point at 350 K, a radial or splayed "hedgehog" equilibrium structure was observed. This structure appears to give the minimum free energy configuration consistent with homeotropic alignment at the liquid-vapor interface and planar alignment at the liquid-surface interface.

ACKNOWLEDGMENTS

The authors wish to thank the EPSRC and British Council for financial support through a grant and studentship, respectively. They are grateful to Professor M. P. Allen for helpful discussions and for generous assistance with computer time, and to Dr. D. R. Binger for computational support.

[1] A. J. McDonald and S. Hanna, J. Chem. Phys. **124**, 164906 (2006).
[2] L. Leger, M. Erman, A. M. Guinet-Picard, D. Ausserre, and C. Strazielle, Phys. Rev. Lett. **60**, 2390 (1988).
[3] F. Heslot, A. M. Cazabat, and P. Levinson, Phys. Rev. Lett. **62**, 1286 (1989).
[4] F. Heslot, A. M. Cazabat, P. Levinson, and N. Fraysse, Phys. Rev. Lett. **65**, 599 (1990).
[5] P. G. de Gennes and A. M. Cazabat, C. R. Acad. Sci., Ser. II: Mec., Phys., Chim., Sci. Terre Univers **310**, 1601 (1990).
[6] M. J. de Ruijter, T. D. Blake, and J. de Coninck, Langmuir **13**, 2164 (1997).
[7] M. J. de Ruijter and J. de Coninck, Langmuir **13**, 7293 (1997).
[8] M. J. de Ruijter, T. D. Blake, and J. de Coninck, Langmuir **15**, 7836 (1999).
[9] S. Bardon, R. Ober, M. P. Valignat, F. Vandenbrouck, A. M. Cazabat, and J. Daillant, Phys. Rev. E **59**, 6808 (1999).
[10] C. Poulard and A. M. Cazabat, Langmuir **21**, 6270 (2005).
[11] J. X. Yang, J. Koplik, and J. R. Banavar, Phys. Rev. Lett. **67**, 3539 (1991).
[12] J. X. Yang, J. Koplik, and J. R. Banavar, Phys. Rev. A **46**, 7738 (1992).
[13] J. A. Nieminen, D. B. Abraham, M. Karttunen, and K. Kaski, Phys. Rev. Lett. **69**, 124 (1992).
[14] J. D. De Coninck, U. D'Ortona, J. Koplik, and J. R. Banavar, Phys. Rev. Lett. **74**, 928 (1995).
[15] S. Bekink, S. Karaborni, G. Verbist, and K. Esselink, Phys. Rev. Lett. **76**, 3766 (1996).
[16] E. A. Müller, I. Rodríguez-Ponce, A. Oualid, J. M. Romero-Enrique, and L. F. Rull, Mol. Simul. **29**, 385 (2003).
[17] M. Yoneya and Y. Iwakabe, Liq. Cryst. **18**, 45 (1995).
[18] M. Yoneya and Y. Iwakabe, Liq. Cryst. **21**, 347 (1996).
[19] D. R. Binger and S. Hanna, Liq. Cryst. **26**, 1205 (1999).
[20] D. R. Binger and S. Hanna, Liq. Cryst. **28**, 1215 (2001).
[21] A. J. McDonald and S. Hanna, Mol. Cryst. Liq. Cryst. **413**, 135 (2004).
[22] S. J. Weiner, P. A. Kollman, D. A. Case, U. C. Singh, C. Ghio, G. Alagona, S. Profeta, and P. Weiner, J. Am. Chem. Soc. **106**, 765 (1984).
[23] C. W. Cross and B. M. Fung, J. Chem. Phys. **101**, 6839 (1994).
[24] J. D. Wright, *Molecular Crystals*, 2nd ed. (Cambridge University Press, Cambridge, 1995).
[25] A. J. Leadbetter, J. L. Durrant, and M. Rugman, Mol. Cryst. Liq. Cryst. Lett. **34**, 231 (1977).
[26] S. Nosé, J. Chem. Phys. **81**, 511 (1984).
[27] W. G. Hoover, Phys. Rev. A **31**, 1695 (1985).
[28] H. J. C. Berendsen, J. P. M. Postma, W. van Gunsteren, A. DiNola, and J. R. Haak, J. Chem. Phys. **81**, 3684 (1984).
[29] W. Smith and T. Forester, J. Mol. Graphics **14**, 136 (1996).
[30] M. T. Downton and S. Hanna, Europhys. Lett. **74**, 69 (2006).

[31] H. Kasten and G. Strobl, J. Chem. Phys. **103**, 6768 (1995).

[32] M. Tintaru, R. Moldovan, T. Belca, and S. Frunza, Liq. Cryst. **28**, 793 (2001).

[33] E. A. Desloge, *Classical Mechanics* (Wiley-Interscience, New York, 1982).

[34] A. Clarke, T. D. Blake, K. Carruthers, and A. Woodward, Langmuir **18**, 2980 (2002).